Electronic Supplementary Information

Unconventional Janus Properties of Enokitake-Like Gold Nanowire Films

Yan Wang[†, δ], Shu Gong[†, δ], Daniel Gómez[§], Yunzhi Ling[†], Lim Wei Yap[†], George. P. Simon[‡, ‖], Wenlong Cheng*[, †, ‡, ⊥]

†Department of Chemical Engineering, Monash University, Clayton, Victoria 3800, Australia;

[‡]New Horizon Research Centre, Monash University, Clayton, Victoria 3800, Australia;

[§]Applied Chemistry and Environmental Sci, RMIT University, Melbourne VIC 3000. Australia;

[‖]Department of Materials Science and Engineering, Monash University, Clayton, Victoria 3800, Australia;

[⊥]The Melbourne Centre for Nanofabrication, Clayton, Victoria 3800, Australia

[δ] *Both authors contributed equally to this manuscript*

*Correspondence author. Email: W. L. Cheng (wenlong.cheng@monash.edu)

This PDF file includes:

- Materials and Methods
- Supplementary Text
- Section S1-S7
- Figures S1-S14
- References

Other Supplementary Material for this manuscript includes the following:

- Movies S1. Free standing Janus gold film in water
- Movies S2. Adhesion test of head and tail side-bonded Janus gold film on Ecoflex

Section S1-S7

Section S1. Fabrication and characterization of standing gold nanowire Janus films

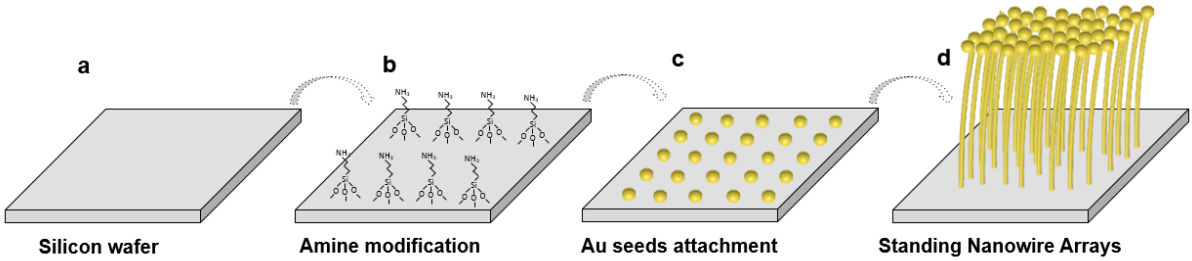

Figure S1. Schematic illustration of the fabrication process of standing gold nanowire-based films on Si wafter surface. (a) A Silicon wafer substrate; (b) surface modification with amine moieties; (c) attachment of citrate-stabilized colloidal gold particle seeds; (d) seed-mediated growth of standing gold nanowire films.

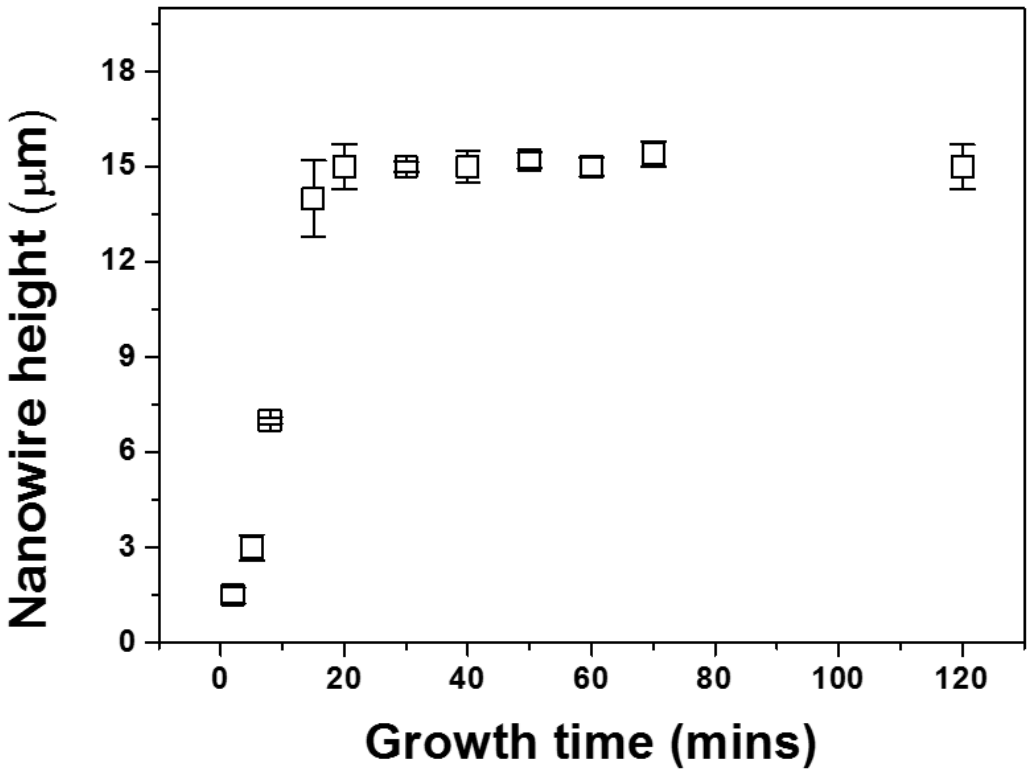

Figure S2. Change of nanowire height as a function of growth time.

Section 2. Janus optical properties

One of the most striking features of our gold Junus film is the fact that it reflects light in a way akin to bulk gold on the "head" side, whilst it displays high (near-complete) absorption of light in the "tail" side. The simplest way to conceptualise the observed near-perfect absorption of the tail side, is to resort to Fresnel's law of reflection,[1] which states that the reflectance R for a normally incident beam of light from a medium characterised with a refractive index n_{inc} (for air $n_{inc} \approx 1$), onto a surface of refractive index n_s is given by:

$$R = \left(\frac{n_s - n_{inc}}{n_s + n_{inc}}\right)^2 \qquad (1),$$

which clearly approaches $R = 0$ (i.e. perfect absorption, since $A = 100\% - R$) as the refractive index of the surface matches that of the incident medium (or $n_s \to n_{inc}$ in the equation). In our materials, this refractive index matching originates due to the spatial sparseness of the gold nanowires on the absorbing (tail) side. According to Fig. 2a (which shows a high-resolution electron micrograph of the absorbing side), each gold nanowire has a diameter of 7.8 ± 1.7 nm and the surface has a number density of ~1.09×10^4 μm^{-2} (based on SEM observation), implying that the average refractive index is close to that of the material in the void between them (i.e. air). Furthermore, the image also shows that this surface is flat and uniform, despite its sparseness, consequently leading to an effective homogeneous surface with respect to its interaction with light (which thus affirms the adequacy of using Fresnel's law of reflection). A similar argument has been developed for explaining the high optical absorbances measured for disordered arrays of carbon nanotubes[2] and for "black gold".[3]

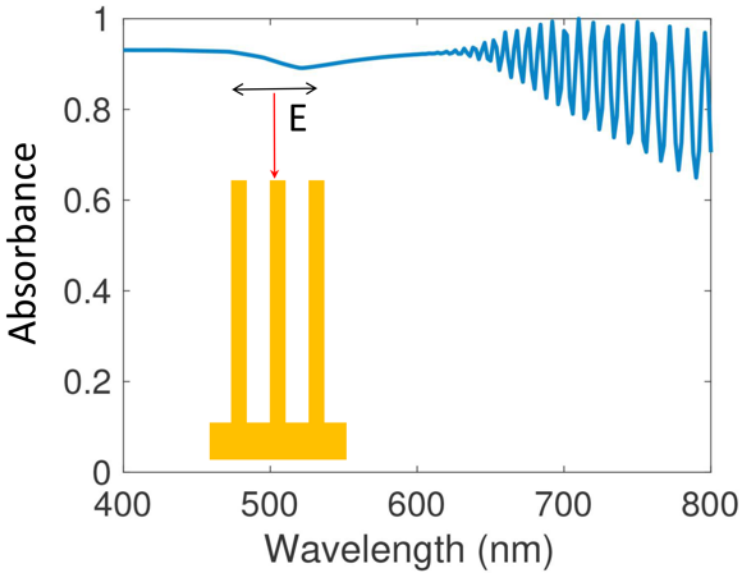

Figure S3. The absorbance from arrays of gold cylinders under wavelength of 400 nm to 800 nm.

In order to gain further insight, we modelled our material as a one-dimensional, periodic array of vertically oriented wires (shown in the above figure to the left) using a Fourier-Modal Method.[4-7] This geometry allows us to understand the effect of the cross-sectional geometry of the structure on the measured optical properties, but it clearly does not represent the complex three-dimensional and disordered nature of the nanowire arrays shown in Figure 2a. The figure to the left shows the calculated absorption spectrum for a nanowire array with a period ≈ 1.6 times the nanowire width. The light was normally incident light with its electric field polarised on the plane of incidence. In agreement with our discussion above, the calculated absorbance is >80% for most of the wavelength range considered. The calculated spectrum shows strong oscillations for wavelengths >650 nm, which occur as a consequence of the assumed periodicity of the modelled structure. In our systems, there is no fixed period as the nanowires form disordered arrays and, consequently, these oscillations are absent in the experimental data. However, the results of the model one-dimensional structure can be almost perfectly superimposed to the measured absorption spectrum, providing strong evidence to support our claim that the high measured absorbance (or near-perfect absorption of light) occurs as a consequence of the refractive index matching discussed in relation to equation (1).

Section S3. Janus wetting properties

Water contact angle of tail-sided film:

The tail side contains standing nanowires and air, which is in essence heterogeous. The appearent contact angle θ* can be predicted by the known Cassie–Baxter equation[8]:

$$\cos\theta^* = -1 + \phi(\cos\theta + 1) \quad (2)$$

Where ϕ is the solid surface fraction and θ is the equilibrium contact angle obtained on a smooth surface of the same chemical composition. The the solid fraction ϕ can be estimated from the nanowire diameter and its number density[9]:

$$\phi = n\pi r^2 \quad (3)$$

Where r is the nanowire radius and n the nanowire number density, which have been estimated to be 3.9 nm and 1.09×10^4 μm^2 (estimation based on SEM observation), respectively. Thus we can yield a solid fraction ϕ of 0.52 from Equation (3). The contact angle of a flat gold surface is 70˚. With those valudes, we can solve equation (2) giving the apparent contact angle of 107.5˚. This is in good agreement with the experimental value of 101 ± 8˚.

Water contact angle of head-sided film:

The head side of Janus film is composed of closely-packed nanoparticles which behaves like a bulk gold film. However, the experimentally estimated contact is ~ 21˚, which is much lower than a smooth gold surfaces. This indiciates MBA molecules must form a self-assembled monolayer on gold nanoparticle surfaces via robust Au-S covalent bonds. This enables exposure of MBA carboxyl moieties to water, hence, rendering the head-sided films highly hydrophilic.

Contact angle under stretched state (50% strain):

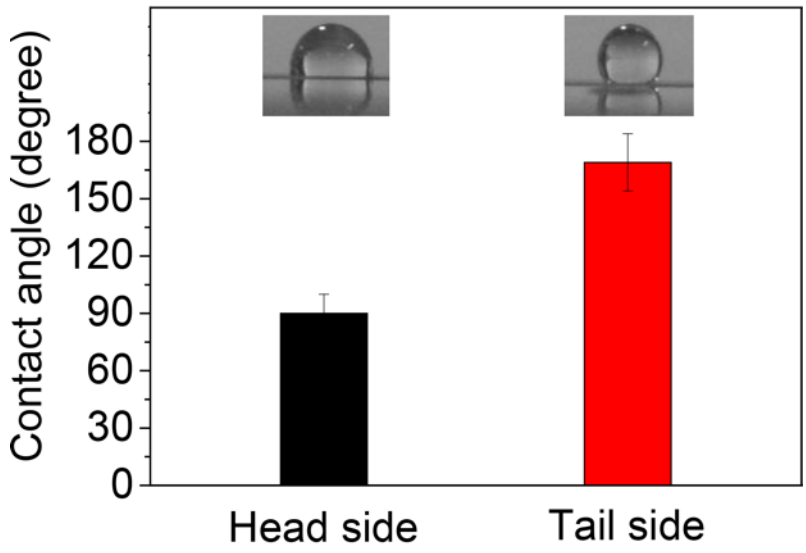

Figure S4. Wettability of Ecoflex bonded head side and tail side enokitake gold film under 50% strain. Films are obtained with 5 mins growth time.

Section S4. Janus conductivities

We investigate the variation in nanowire height to the resistance of film by extending a simple model of Volger.[10-11] In this model, nanowires are assumed to be consisted of stacking cubes depending with the edge size 'a'. The height of nanowires is determined by the number of cubes as shown in Figure S5, with equal spacing between the neighbouring nanowires. We further assume the inter-cube distances along z direction is 0, while along x and y directions are *t*. The choice of cubical nature of nanowires allows us to take the same cubic resistance 'R_c' and the three axes. To simplify the calculation, the resistivity of the cubes is considered to be the same as that of a single crystal, and hence could be written as:

$$R_c = \rho_c / a \qquad (4)$$

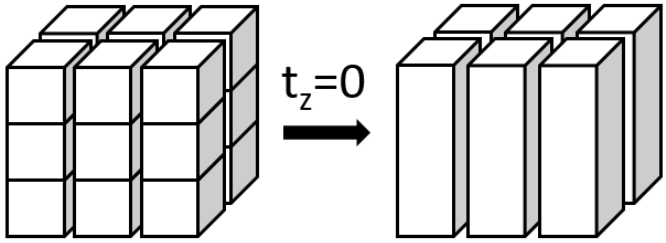

Figure S5. The cube model of our nanowire system

Considering the film of thickness '*d*', length '*l*' and width '*w*', the number of cubes '*q*' along the length '*l*' can be imagined to be arranged regularly at equal inter cube spacing '*t*'. Similarly, '*r*' and '*p*' are cube numbers along the width and thickness of the film. So, the total number of cubes in the film is equal to:

$$n = qpr \qquad (5)$$

Also, from the assumed arrangement of cubes as shown in Fig. S7 we have:

$$d = pa$$
$$l = qa + (q-1)t$$
$$w = ra + (r-1)t \qquad (6)$$

The resistance along the length of the film can be measured by taking the contacts across the cross-section in the yz plane. The equivalent dc circuit of this arrangement of measurement would be as shown in Figure S6, where 'R_b' represents the high resistance of the inter-grain voids which is a function of '*t*' which in turn would depend on the mechanism by which charge carriers would cross the inter-cube boundary.

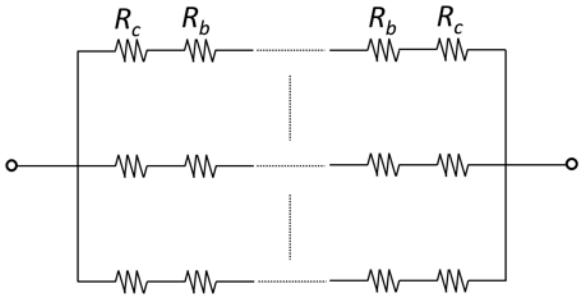

Figure S6. Equivalent dc circuit of the cubic arrangement nanowires.

As can be seen in Fig. S8, the whole film can be considered to be a parallel combination of *'pr'* resistive elements, where resistance of each element is given by

$$R = qR_c + (q-1)R_b \qquad (7)$$

Thus, the net resistance along the length of the film between the two contacts would be given as:

$$R_{net} = \frac{qR_c+(q-1)R_b}{pr} \qquad (8)$$

Substituting equation (6), we get

$$R_{net} = \frac{(\frac{l+t}{a+t})\frac{\rho_c}{a}+(\frac{l-a}{a+t})R_b}{\frac{d}{a}(\frac{w+t}{a+t})} \qquad (9)$$

In general, the inter-cubic resistance R_b is quite higher than the cube resistance R_c. R_b may be written as $\rho_c f(t)t/a^2$. The function $f(t)$, would depend on the mechanism of charge transfer between the two neighbouring cubes. There eq (6) maybe written as

$$R_{net} = \frac{\rho_c}{d(w+t)}[l + t + (l-a)f(t)\frac{t}{a}] \qquad (10)$$

In our case it is quite reasonable to apply the condition $l >> a$, $l >> t$ and $w >> t$ above. Then, equation (5) reduces to

$$R_{net} = \frac{l\rho_c}{dw}(1 + f(t)\frac{t}{a}) \qquad (11)$$

Based on our SEM observation, each gold nanowire and nanoparticle have a diameter of 7.8 ± 1.7 nm and 9.3± 2.1 nm, respectively. We estimate a=7.8 nm and t=1.5 nm. We measured the resistance of back side film with l=w=10 mm and ρ_{Au}=2.6 ×10^{-8} m Ω (T=20˚C). The experiment result is well fitting to theoretical calculation when $f(t)$=15,000.

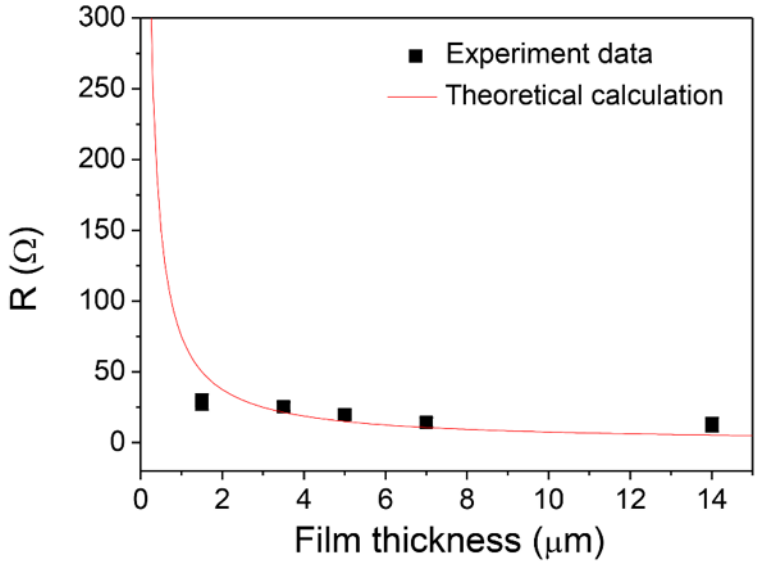

Figure S7. The experiment data of film thickness as a function of resistance and the theoretical calculation result.

Section S5. Janus stretchability

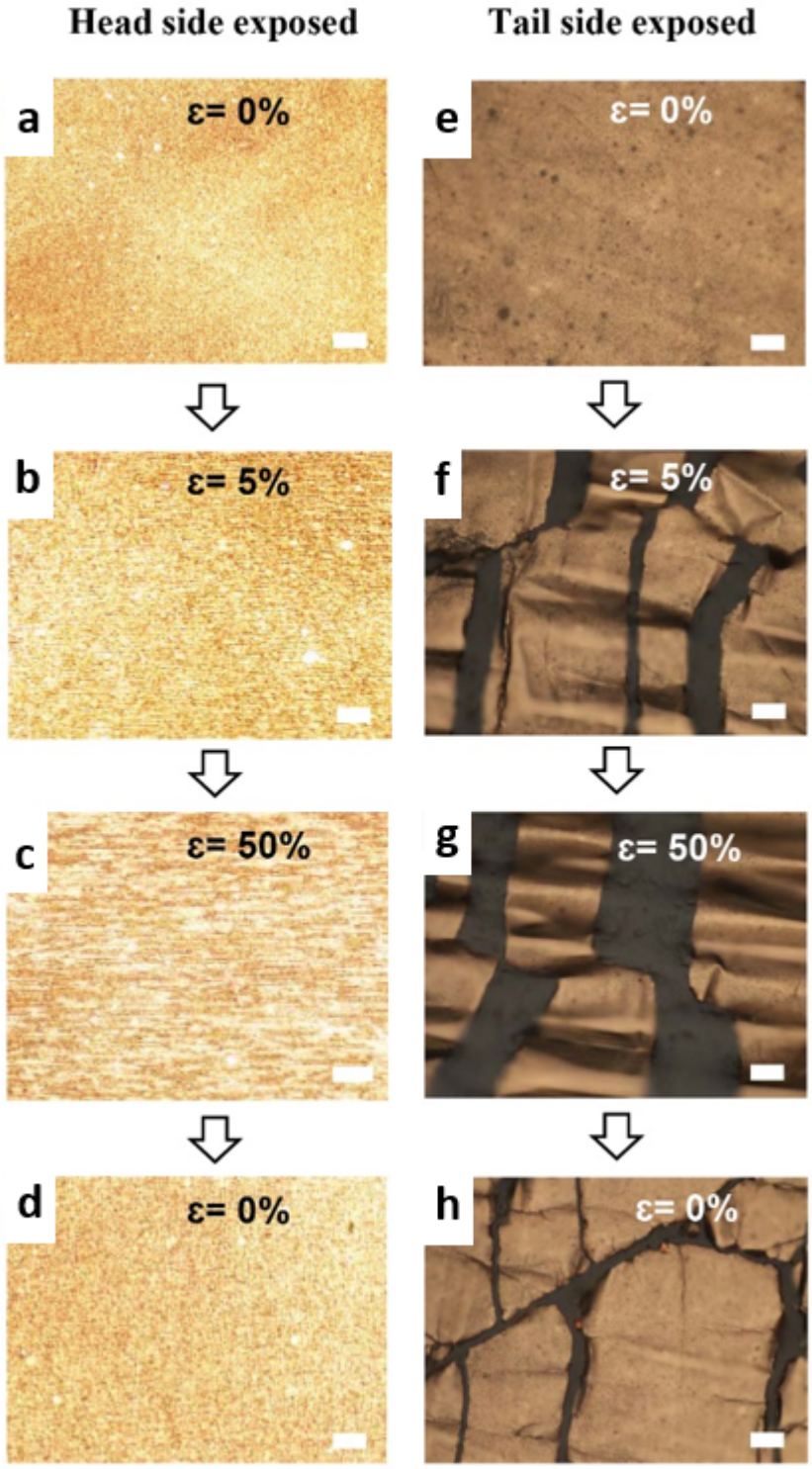

Figure S8. Optical images of the surface morphological changes of gold Janus films bonded to Ecoflex under different levels of tensile strains (0%-5%-50%-0%). (a-d) head side exposed film; (e-h) tail side exposed film. Films are obtained with 3 minutes growth time. Scale bar: 20 μm. Stretching strain is performed horizontally.

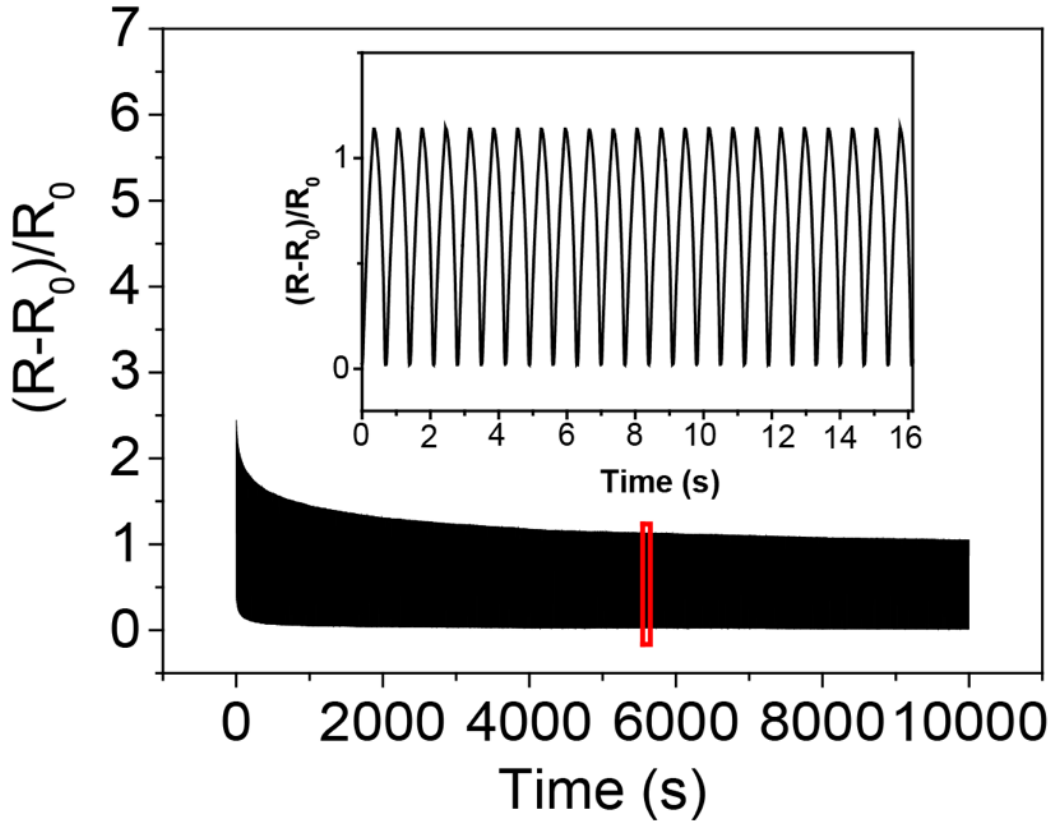

Figure S9. Cycling test (~15,000 cycles) of tail-bonded film under strain of 80%. Nanowire height: 1.5 μm.

Section S6. Janus bending sensitivity

The bending sensitivity may be defined as

$$S = \theta(R_{bending} - R_0)/R_0 \qquad (12)$$

Where R_0 is the original resistance of film before bending, $R_{bending}$ is the resistance of film with bending and θ is applied bending degree.

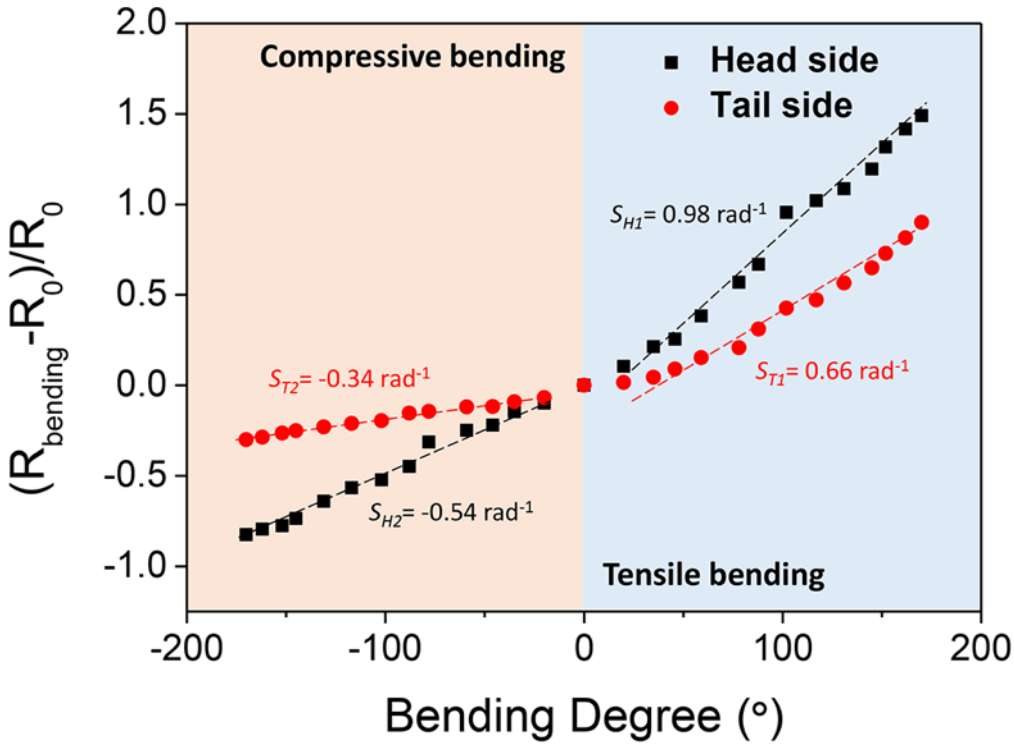

Figure S10. The resistance changes as a function of bending degree during compressive and tensile bending of standing enokitake nanowire-based Janus film with both head side (black) and tail side (red) on top.

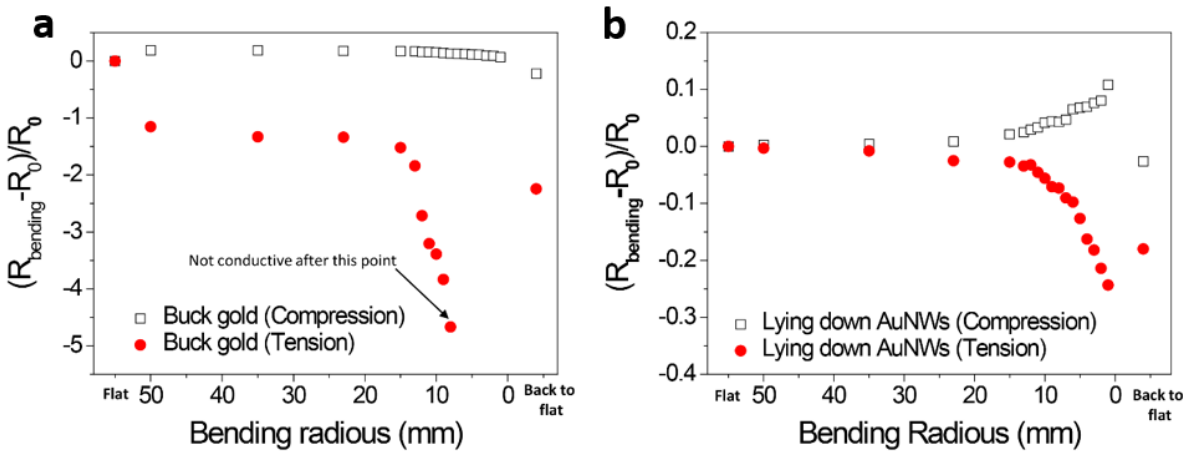

Figure S11. The resistance changes of an evaporated gold film and lying down gold nanowire film during compressive and tensile bending with radious up to 1 mm. (a) Evaporated Gold film; (b) Lying-down gold nanowire film.

Section S7. Discrimination of external point loads

The point load sensitivity may be defined as

$$S = F(R_{load} - R_0)/R_0 \qquad (13)$$

Where F is the point load and R_{load} is the resistance of film with point load.

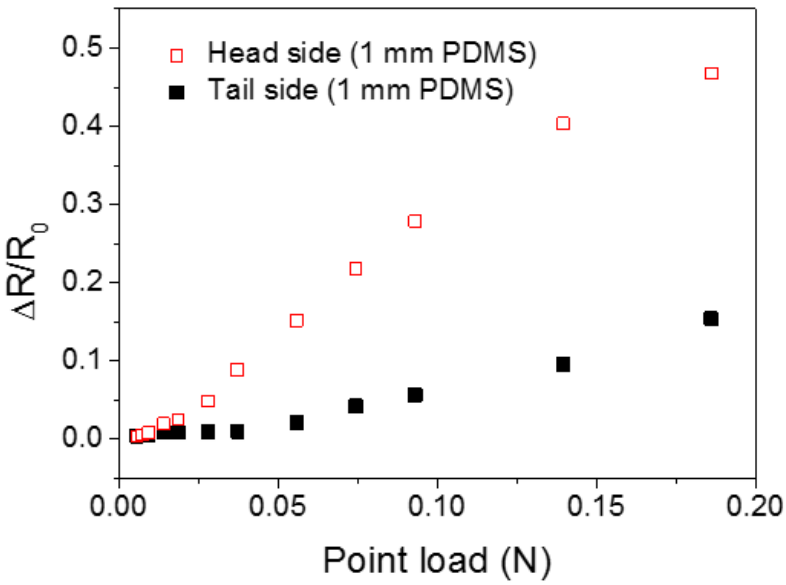

Figure S12. The resistance changes as a function of point load from 0 to 0.2 N. Free-standing gold nanowire film is transferred onto 1 mm thick PDMS sheet with head side exposed (red hollow square) and tail side exposed (black square).

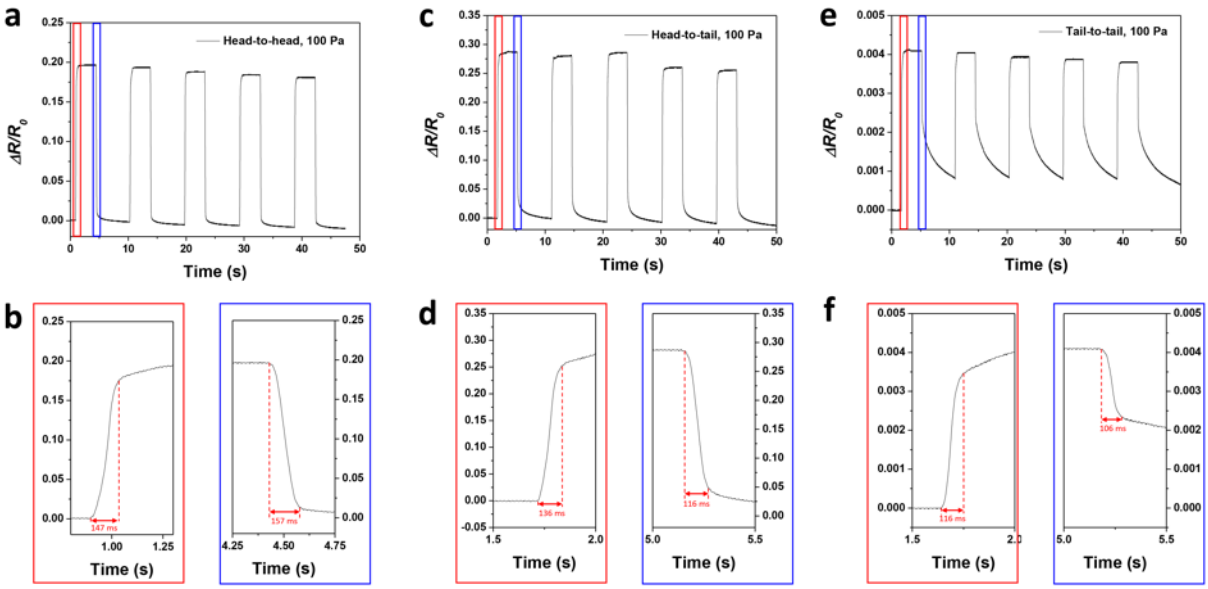

Figure S13. (a), (c) and (e) are the resistance changes of enokitake-like gold nanowire pressure sensors under repeated pressure of 100 Pa based on head-to-head (a), head-to-tail (c), and tail-to-tail (e) layout, respectively. (b), (d), and (f) are enlarged figures of (a), (c), and (e) to estimate the response time of both loading and unloading process.

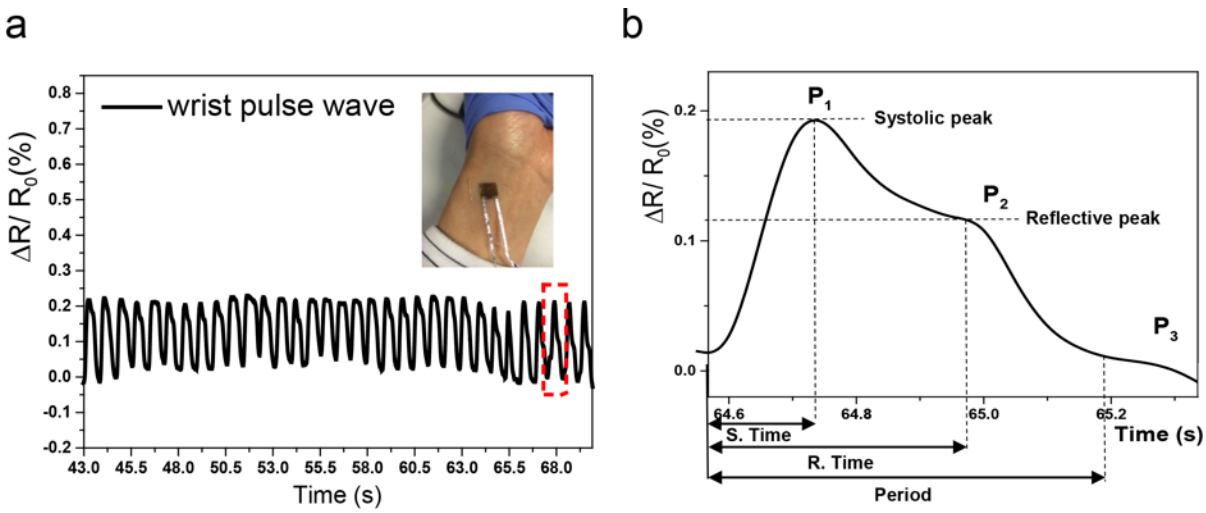

Figure S14. Real time wrist pulse wave could be detected by enokitake-like gold nanowire pressure sensor. (a) Electrical responses for pulse wave. (b) Enlarged figure of one particular pulse wave.

References

1. Griffiths, David J., and R. Colleger. *Introduction to Electrodynamics*, prentice Hall Upper Saddle River." *New Jersey* 7458 (1999).
2. Mizuno, K., Ishii, J., Kishida, H., Hayamizu, Y., Yasuda, S., Futaba, D.N., Yumura, M. and Hata, K. A Black Body Absorber From Vertically Aligned Single-Walled Carbon Nanotubes. *Proc. Natl. Acad. Sci. U.S.A* **106**, 6044 (2009).
3. Ng, C., Yap, L.W., Roberts, A., Cheng, W. and Gómez, D.E. Black Gold: Broadband, High Absorption of Visible Light for Photochemical Systems. *Adv. Funct. Mater.* **27**, 1604080 (2016).
4. Thongrattanasiri, S., Koppens, F. H. L., and García de Abajo, F. J. Complete Optical Absorption in Periodically Patterned Graphene. *Phys. Rev. Lett.* **108**, 047401 (2012).
5. Lalanne, P., Jurek, M. P. Computation Of The Near-Field Pattern with the Coupled-Wave Method for Transverse Magnetic Polarization. *Modern Opt.* **45**, 1357-1374 (1998).
6. Lalanne, P. & Morris,G. M. Highly Improved Convergence of the Coupled-Wave Method for TM Polarization. *Opt. Soc. Am. A* **13**, 779-784 (1996).
7. Moharam, M.G., Grann, E.B., Pommet, D.A. and Gaylord, T.K. Formulation for Stable and Efficient Implementation of the Rigorous Coupled-Wave Analysis of Binary Gratings. *Opt. Soc. Am. A* **12**, 1068-1076 (1995).
8. Abdelsalam, M.E., Bartlett, P.N., Kelf, T. and Baumberg, J. Wetting of Regularly Structured Gold Surfaces. *Langmuir* **5**, 1753-1757 (2005).
9. Lau, K.K., Bico, J., Teo, K.B., Chhowalla, M., Amaratunga, G.A., Milne, W.I., McKinley, G.H. and Gleason, K.K. Superhydrophobic Carbon Nanotube Forests. *Nano Lett.* 12, 1701-1705 (2003).
10. Volger, J. Note on the Hall Potential Across An Inhomogeneous Conductor. *Phys. Rev.* **79**, 1023 (1950).
11. Arun, P., Tyagi, P. A., Vedeshwa, G. R. Large Grain Size Dependence of Resistance of Polycrystalline Films. *Phys. B Condens. Matter.* **322**, 289-296 (2002).